

Properties of microemulsions with sugar surfactants and peppermint oil

Monzer Fanun

Received: 13 January 2009 / Revised: 25 March 2009 / Accepted: 20 April 2009 / Published online: 12 May 2009
© Springer-Verlag 2009

Abstract In this study, we report on the properties of water + propylene glycol/sugar surfactant/peppermint oil + ethanol. The sugar surfactants were sucrose monolaurate and sucrose dilaurate. The mixing ratios (w/w) of water/propylene glycol and that of ethanol/oil equal 2 and 1, respectively. U-type microemulsions were observed in the sucrose monolaurate while S-type microemulsions were observed in the dilaurate-based systems. Temperature-insensitive microemulsions were formulated using the two surfactants. Water volume fraction percolation thresholds were determined by the study of electrical conductivity and dynamic viscosity. The structural parameters that include the periodicity and the correlation length were estimated using small angle X-ray scattering. The periodicity increases linearly with the increase in the water content whereas the correlation length increases with the increase in the water volume fraction to a certain value then decreases. The diffusion properties investigated by nuclear magnetic resonance confirm a progressive transformation of the microemulsions from water-in-oil to bicontinuous and inversion to oil-in-water upon dilution with water. The hydrodynamic radius of diluted microemulsions measured by dynamic light scattering increases with the increase in temperature. The area per polar head group decreases with the increase in temperature.

Keywords Percolation threshold · Periodicity · Correlation length · Diffusion coefficients · Hydrodynamic radius

Introduction

Microemulsions are spontaneously forming, thermodynamically stable, homogeneous low viscous, and optically isotropic solutions. Microemulsions are composed from water, oil, and surfactant and in many cases a cosurfactant or cosolvent is added to permit encapsulating large amounts of water [1–4]. Due to their unique properties, microemulsions have been used in a variety of technological applications, including environmental protection, nanoparticle formation, food product formulations, delivery systems, separation medium, and chemical and biochemical reaction media [1, 5]. The placement of the solubilized oil in the surfactant aggregates highly affects the change in surfactant layer curvature. In previous studies [6–8], we reported on microemulsions formulation using cyclic hydrocarbons. These oils influence the surfactant layer curvature in aggregates or self-organized structures when solubilized. If oil tends to penetrate in the surfactant palisade layer and locates near the interface of the water–lipophilic surfactant moiety, the curvature would be less positive or negative [9, 10]. It is known that cyclic hydrocarbons tend to penetrate in the surfactant layer and widen the effective cross-sectional area per surfactant. As a result, the surfactant layer curvature becomes less positive or negative. Extensively studied [11–16], the phase behavior of sucrose ester surfactants in water and oil demonstrated that in many industrial applications the use of these nonionic surfactants system is preferred for many food, cosmetics, and pharmaceutical applications [13–16]. A number of factors

Electronic supplementary material The online version of this article (doi:10.1007/s00396-009-2043-y) contains supplementary material, which is available to authorized users.

M. Fanun (✉)
Colloids and Surfaces Research Laboratory Faculty of Science
and Technology, Al-Quds University,
P.O. Box 51000, East Jerusalem, Palestine
e-mail: Fanunm@gmail.com
e-mail: mfanun@science.alquds.edu

influence water solubilization in nonionic surfactants/oil mixtures [17–19]. The comprehensive view of the physicochemical properties and microstructures of microemulsions requires the use of a variety of experimental methods [20]. Microemulsions are fluids that exhibit diverse and complex dynamics, which are dependent on the system thermodynamics (i.e., composition and the resulting microstructure), and the dynamics of the constituent molecules [1–4]. The structure of microemulsions can be idealized as a set of interfaces dividing polar and apolar domains. Mixtures of water, oil, and surfactant exhibit a rich variety of microstructures, ranging from spherical micelles, rod-like micelles, and bicontinuous microemulsions to ordered liquid crystalline phases. So far, with increasing water volume fraction, discrepancies with respect to the hard sphere model have been discussed in terms of strong interparticle interactions, microstructural transitions, and percolation behaviors, which are oil- and temperature-dependent [21–23]. In the present work, we report for the first time the study of the formation, transport, microstructure, and diffusion properties of sucrose ester and peppermint oil (MNT)-based microemulsions. These microemulsion systems are intended for the use in solubilizing food flavors, pharmaceutical active ingredients, and cosmetic ingredients. Peppermint oil is edible oil that is suitable for food, pharmaceutical, and cosmetics applications.

Experimental

Materials

The sucrose laurate surfactants used in this study were obtained from Mitsubishi-Kasei Food Corp., (Mie, Japan). Table 1 shows the compositions of these surfactants. Peppermint oil (98%) and 1, 2-propandiol (propylene glycol; $\geq 99.5\%$) were purchased from BDH (Poole, UK). Ethanol (minimum 99.8%) was purchased from Sigma Chemicals Co. (St. Louis, USA). Sodium chloride of analytical grade was purchased from J.T. Baker Inc. (Phillipsburg, USA). All of the components were used as supplied without further purification. Triple distilled water was used.

Methods

Pseudoternary phase diagrams at constant temperature

The phase behavior of a system consisting of water, oil, surfactant, and cosurfactant may be described on a phase tetrahedron whose apexes respectively represent the pure components. However, it is more convenient to describe the phase behavior on pseudoternary phase triangles. Obviously, a fixed (weight, volume, or mole) ratio must be chosen for any two of the components and one of the triangle vertices represents 100% of this binary mixture. Mixtures at fixed weight ratios of oil, surfactant, and ethanol were prepared in culture tubes sealed with Viton-lined screw caps. Water and propylene glycol were then added dropwise until its solubilization limit was reached. After this point, larger increments of aqueous phase were added. Vigorous stirring followed all of the aqueous phase additions on a vortex mixer. The time for equilibration between additions of successive aliquots was typically, from a few minutes up to 24 h. Phase transitions detected visually by the appearance of cloudiness or sharply defined separated phases. The completion of this process was hastened by centrifuging the samples. The phase diagrams were determined at 25 ± 0.5 °C.

Electrical conductivity measurements

Conductivity measurements were performed at 25 ± 0.5 °C on samples, the compositions of which lie along the one-phase channel, using a conductivity meter: the conductivity cell used is Tetra Con® 325, the electrode material is graphite, and the cell constant is $0.475 \text{ cm}^{-1} \pm 1.5\%$. The range of application is between $1 \mu\text{S/cm}$ and 2 S/cm with an accuracy of $\pm 0.5\%$, and the temperature range is from -5 to 100 °C. In the case of nonionic microemulsions, a small amount of an aqueous electrolyte must be added for electrical conduction [24]. Thus, a 0.01-M sodium chloride aqueous solution was used in the preparation of the microemulsion samples in place of pure water. The electrode was dipped in the microemulsion sample until equilibrium was reached and reading becomes stable. Reproducibility was checked for certain samples and no

Table 1 Type and composition of sucrose esters used in this research project

Type	HLB	Purity of combined fatty acid (%)	Ester composition (%)		Melting temperature (°C)	
			Monoester	Di, tri and polyester	Start point	Peak point
Sucrose monolaurate (L1695)	16	Lauric 95	80	20	35	47
Sucrose dilaurate (L595)	5	Lauric 95	30	70	35	47

significant differences were observed. The constant of the conductivity cell was calibrated using standard KCl solutions and checked a minimum of three times during the course of the working shift.

Viscosity measurements

Viscosity was measured using a rotational viscometer, model DV-1PL spindle from Anton Paar GmbH (Graz, Austria). “Double cylinder” geometry was used. Viscosities at 200 s^{-1} shear rate were obtained at $25 \pm 0.5\text{ }^{\circ}\text{C}$. Reproducibility (triplicate) was checked for the samples and no significant differences ($\pm\text{SD}$) were observed.

Small angle X-ray scattering

Scattering experiments were performed using Ni-filtered Cu K α radiation (0.154 nm) from an Elliott GX6 rotating X-ray generator that operated at a power rating up to 1.2 kW. X-radiation was further monochromated and collimated by a single Franks mirror and a series of slits and height limits and measured by a linear position-sensitive detector. The sample was inserted into 1–1.5 mm quartz or lithium glass capillaries, which were then flame-sealed. Each sample was checked before and after the experiment to verify that no fluid had been lost during the time of exposure, approximately 3 h. The temperature was maintained at $25 \pm 1\text{ }^{\circ}\text{C}$. The sample-to-detector distance was 0.46 m, and the scattering patterns were measured using the Lake procedure [25].

X-ray data analysis

In this case, the scattering patterns after background subtraction were fit to the expression due to Teubner and Strey [26]:

$$I(q) = (1/a_2 + c_1 q^2 + c_2 q^4) + b \quad (1)$$

With the constants a_2 , c_1 , c_2 , and b obtained by using the Levenburg–Marquardt procedure [27]. Such a functional form is simple and convenient for the fitting of spectra. Equation 2 corresponds to a real space correlation function of the form

$$\gamma(r) = (\sin k r / k r) e^{-r/\xi}. \quad (2)$$

The correlation function describes a structure with periodicity $d = (2\pi/k)$ damped as a function of correlation length ξ . This formalism also predicts the surface to volume ratio, but because this ratio is inversely related to the correlation length and therefore must go to zero for a perfectly ordered system, calculated values are frequently

found to be too low [28]. d and ξ are related to the constants in Eq. 1 by [26]:

$$d = 2\pi \left[(1/2) ((a_2/c_2))^{1/2} - (c_1/4c_2) \right]^{-1/2} \quad (3)$$

$$\xi = \left[(1/2) ((a_2/c_2))^{1/2} + (c_1/4c_2) \right]^{-1/2}. \quad (4)$$

Pulsed gradient spin echo-nuclear magnetic resonance

NMR measurements were performed on Bruker DRX-400 spectrometer with a BGU II [29, 30] gradient amplifier unit and a 5-mm BBI probe equipped with a z-gradient coil, providing a z-gradient strength (G) of up to 55 G cm^{-1} . The self-diffusion coefficients were determined using bipolar-pulsed field gradient-stimulated spin echo. In this work, we used bipolar gradient pulses as described by Wu et al. [29] to reduce the eddy-current effects. Experiments were carried out by varying the gradient strength and keeping all other timing parameters constant. The self-diffusion coefficient (D) is given by

$$I = I_0 \exp \left[\gamma^2 G^2 \delta^2 \left(\Delta - \frac{\delta}{3} \right) D \right] \quad (5)$$

Where I is the measured signal intensity, I_0 is the signal intensity for $G=0$, γ is the gyro magnetic ratio for the ^1H nucleus, δ is the gradient pulse length, and Δ is the time between the two gradients in the pulse sequence (and hence defines the diffusion time). Typically, we use $\Delta=100\text{ ms}$ and $\delta=8\text{ ms}$ and vary G from 1.7 to 32.3 G cm^{-1} in 32 steps.

Dynamic light scattering

Each liquid sample was inserted into a 10-mm diameter borosilicate test tube and centrifuged for 15 min at 3,000 rpm in order to remove dust. The test tube was then placed in a temperature-controlled vat of toluene as the index matching fluid. The light source was an argon ion laser (Spectra Physics-Lexel; $\lambda=514.5\text{ nm}$). Photons scattered by the sample were collected by an ITT PW130 photomultiplier tube mounted at 90° to the incident laser beam. The photoelectron count-time autocorrelation function was calculated with a BI 2030 AT (Brookhaven Instruments) digital autocorrelator and was analyzed using the constrained regularization algorithm, CONTIN [31, 32] to give an intensity-weighted distribution of the translational diffusion coefficients D_z . Particle hydrodynamic size

was calculated from the translational diffusion coefficient using the Stokes–Einstein relationship:

$$D_H = k_B T / 6\pi\eta D_z \quad (6)$$

where D_H is the hydrodynamic diameter, k_B is Boltzmann's constant, T is the absolute temperature, and η is the solvent viscosity. The results are averages of three or four experiments. D_H is obtained from the positions of the peaks of the intensity-weighted size distribution function.

Results and discussion

Phase behavior

The pseudoternary phase diagrams of the water + propylene glycol/sucrose laurate/peppermint oil + ethanol systems were studied at 25, 37, and 45 °C. The mixing ratios (w/w) of water/propylene glycol and that of ethanol/oil equal 1 and 2, respectively. The surfactants were L1695 and L595. Figure 1 presents the pseudoternary phase diagrams for the two surfactants. The phase behavior indicates the presence of an isotropic and low-viscosity area that is a microemulsion one-phase region (1ϕ), the remainder of the phase diagram represents a two-phase region composed of water continuous micellar solution with excess oil designated by (Wm+O). Generally, it is always considered that within this two-phase region, a microemulsion phase (if it is transparent) exists in equilibrium with an excess oil phase when the oil content is high, or an emulsion phase (if it is turbid) exists in equilibrium with an excess oil phase. The total area (A_T) of the microemulsion region observed in these systems increases slightly as a function of temperature indicating that sucrose esters form temperature-insensitive microemulsions in the presence of peppermint oil (see Fig. 1 in [Electronic supplementary material](#)). Similar results on the formation of temperature-insensitive sucrose esters microemulsions were reported [5, 33]. Compared to the ternary system reported in our previous study [34], adding ethanol and propylene glycol to the water/sucrose laurate/peppermint oil ternary mixture enhances the area of the one-phase microemulsion in the systems based on the two surfactants. The presence of alcohol and/or glycol influences the extent of the microemulsion regions and their internal structure. The roles of alcohol or glycol in microemulsions are (1) to delay the occurrence of liquid crystalline phases, (2) to increase the fluidity of the interfacial layer separating oil and water, to decrease the interfacial tension between the microemulsion phase and excess oil and water, and (3) to increase the disorder in these interfacial layers as well as their dynamic character. Other authors [17, 35–39] reported on the effect of ethanol

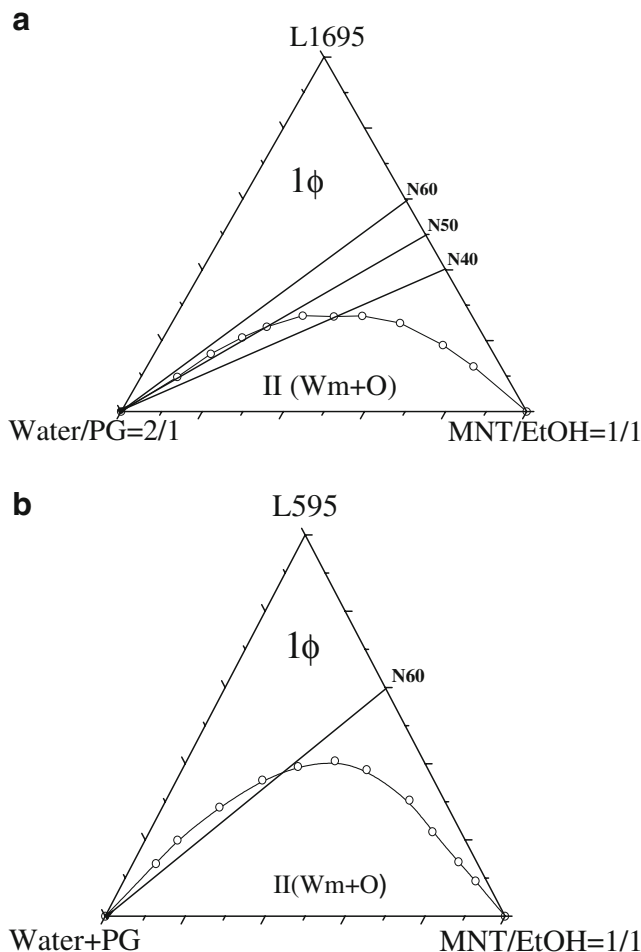


Fig. 1 Pseudoternary phase behavior of the water + propylene glycol/sucrose laurate/peppermint oil + ethanol system at 25°C. The mixing ratios (w/w) of water/propylene glycol and that of ethanol/oil equal 2 and 1, respectively. The one-phase region is designated by 1ϕ , and the two-phase region consisted of water continuous micellar solution with excess oil designated by Wm+O. N60 is the water dilution line where the weight ratios of sucrose monolaurate/peppermint oil/ethanol equal to 3:1:1. **a** L1695, **b** L595

and propylene glycol on the enhancement of the water solubilization in nonionic surfactants and oil when added.

Thermodynamics of solubilization

Solubilization of either water in surfactant/oil medium or oil in water/surfactant medium up to the phase separation point leading to the formation of water-in-oil or oil-in-water microemulsions can be considered the limit of maximum solubility of the dispersing phase. The corresponding free energy of dissolution (G_s^0) at a constant temperature can be obtained from the relation [4]

$$\Delta G_s^0 = -RT \ln X_d \quad (7)$$

where X_d is the mole fraction of the dispersed phase (either oil or water) and R is the gas constant. Since the dispersed

phase existed in the form of surfactant-coated droplets, it would be more appropriate to consider X_d as the mole fraction of the dispersed droplets. Knowledge of the droplet size was required to estimate X_d . The estimation of ΔG_s^0 herein reported was done based on mole fraction of dispersed water or oil. The free energy of solubilization (ΔG_s^0) for both oil-in-water and water-in-oil microemulsions studied were calculated. It was found that the ΔG_s^0 values were positive and decrease as the water content increases in the water-in-oil microemulsions indicating that adding water to the water-in-oil microemulsions disrupts their organization. The oil-in-water microemulsions yielded ΔG_s^0 values higher than the water-in-oil microemulsions and increases with the increase in the water content. The dispersed droplets of either water or oil are surrounded by a layer of surfactant in the continuous medium in an organized state. The oil-dispersed system is more stabilized and organized than the water-dispersed case.

Transport properties

Electrical conductivity

The electrical conductivity was measured on the (water + propylene glycol + sodium chloride)/sucrose laurate/peppermint oil + ethanol along the dilution line N60 at 25 °C. The concentration of sodium chloride in water is 0.01 M. All samples appeared transparent and isotropic. It is possible to measure the conductivity of the microemulsion stabilized by nonionic surfactants without the addition of a small amount of salt if they contain little ionic impurities, but the amount of added electrolyte is very low that it is negligible and does not affect the extent of the one-phase microemulsion region nor the microemulsion properties. The influence of water volume fraction change on the electrical conductivity σ with respect to volume fraction of water is shown in Fig. 2. With the increase in the water volume fraction, the electrical conductivity increases exponentially in all systems studied. The microstructure of water-in-oil microemulsions is reasonably well described in terms of spherical droplets [1–4]. So far, with increasing water volume fraction, discrepancies with respect to the hard sphere model have been discussed in terms of strong interparticle interactions, microstructural transitions, and percolation behaviors, which are oil- and temperature-dependent [1–4]. Clusters of droplets which, in turn, generate water networks throughout the water-in-oil phase are produced by the short-range attractive interactions. As a sequence, important changes of the transport properties, such as dynamic viscosity and electrical conductivity, occur. The phenomena have been described in terms of “percolation” [1–4]. According to the percolation model,

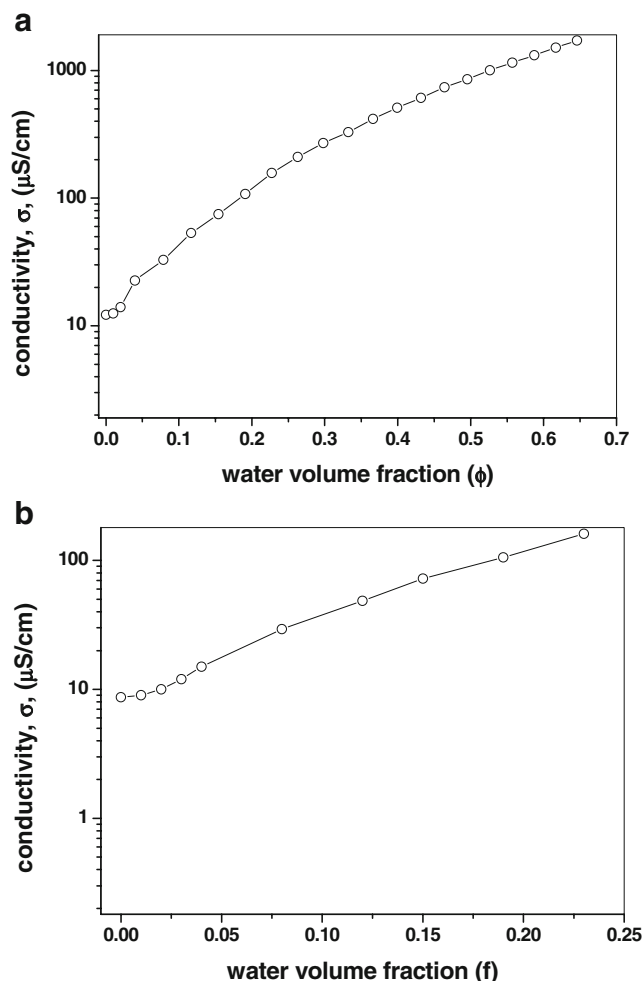


Fig. 2 Variation of the electrical conductivity ($\log(\sigma)$) of (water + propylene glycol + sodium chloride)/sucrose laurate/peppermint oil + ethanol system as function of water volume fraction along the dilution line N60 at 25 °C. The mixing ratios (w/w) of water + propylene glycol and that of ethanol/oil equal 2 and 1, respectively. Sodium chloride concentration in water is 0.01 M. The phase diagrams are presented in Fig. 1. The lines serve as guides to the eye. **a** L1695, **b** L595

the conductivity remains low up to a certain volume fraction (ϕ_c) of water at constant temperature, when the temperature reaches a value T_c at constant water volume fraction ϕ , or when the water-to-surfactant molar ratio increases. It must be emphasized that these conducting water-in-oil droplets below ϕ_c are isolated from each other embedded in nonconducting continuum oil phase and hence contribute very little to the conductance. However, as the volume fraction of water reaches the percolation threshold ϕ_c , some of these conductive droplets begin to contact each other and form clusters which are sufficiently close to each other. The number of such clusters increases very rapidly above the percolation threshold ϕ_c , giving rise to the observed changes of properties, in particular to the increase of electrical conductivity. The electrical

conductivity σ above ϕ_c has been attributed to the transfer of counter ions from one droplet to another through water channels opening between droplets during sticky collisions through transient merging of droplets [4]. The existence and position of this threshold depends on the interactions between droplets which control the duration of the collision and the degree of the interface overlapping, hence the probability of merging. Building up of conductivity needs attractive interactions and ϕ_c decreases when the strength of these interdroplet interactions increases as predicted by recent theoretical calculations [40]. In the present study, a theoretical model of Safran et al. [40], which is based on the dynamical picture of percolation, has been utilized to analyze the conductivity results of the systems. According to the theory

$$\sigma = A(\phi_c - \phi)^{-s} \quad \text{if } \phi < \phi_c \quad (8)$$

$$\sigma = B(\phi - \phi_c)^t \quad \text{if } \phi > \phi_c. \quad (9)$$

The critical exponent t generally ranges between 1.5 and 2, whereas the exponent s allows assignment of the time-dependent percolation regime. Thus, $s < 1$ (generally around 0.6) identifies a “static percolation” regime, and $s > 1$ (generally around 1.3) identifies a “dynamic percolation” regime. The static percolation is related to the appearance of bicontinuous microemulsions [41]. The dynamic percolation [40, 42] is related to rapid processes of fusion–fission among the droplets. Transient water channels form when the surfactants interface breaks down during collisions or through the merging of droplets. The interpretation of these interactions in terms of static or dynamic percolation is obviously strictly dependent on the time-scale of the experimental technique. Experiments carried out within the whole microemulsion phase revealed a variety of interactions upon moving on water dilution line N60. Close to the oil corner, the interactions can be described in terms of charge fluctuations among small w/o droplets. With increasing surfactant and water content, the lifetime of the contacts among the droplets increases up to the identification of a structural transition from closed water domains to a connected water network through a gradual variation of the interconnectivity. These changes have been attributed to the occurrence of a percolation transition [40]. We have determined ϕ_c , s , and t and the prefactors A and B by numerical analysis with adjustment by the least-squares method using simultaneously Eqs. 8 and 9. The computed s and t values indicate that the percolation process is static. The resulting ϕ_c values obtained in this manner are close to the values obtained by the numerical estimate of the maximum of $(d \log \sigma / d \phi)$ versus ϕ (see Fig. 2 in [Electronic supplementary materials](#)). There is a reasonable agreement

between calculated (by Eqs. 8 and 9) and experimental values within prescribed range of composition with a mean deviation of 4%. The above equations are valid only near ϕ_c and cannot be extrapolated to infinite dilution and unit concentration. In addition, these are not applicable at the immediate vicinity of ϕ_c , where there is a continuous variation within a narrow interval around the percolation threshold.

Dynamic viscosity

The study of the dynamic viscosity of microemulsions can provide information on the intrinsic and derived processes in the microemulsion system, as well as furnish knowledge on the overall geometry of the particles of the dispersed phase [4, 43, 44]. Viscosity measurements evidenced the dependence of the size and shape of microemulsion droplets on the amount of solubilized water. The understanding of the structural consistencies in microemulsions has also been attempted from viscosity measurements by others [45, 46]. Figure 3 shows the variation in the dynamic viscosity as function of water volume fraction in the water + propylene glycol/sucrose laurate/peppermint oil + ethanol systems for L1695 and L595 along the dilution line N60. The gradual decrease of viscosity that began at water volume fractions above the ϕ_c obtained by the electrical conductivity results indicates the interrelation between the dynamic viscosity and the electrical viscosity of these systems. The range of water volume fraction above ϕ_c is decomposed in four different regions. Region 1 where the water volume fractions are between ϕ_c and $\phi < 0.2$ suggests that the percolated droplets are gradually transferring to bicontinuous structure at $\phi = 0.2$, where the bicontinuous structure is fully developed (region 2 where $0.2 < \phi < 0.37$). The inversion of the bicontinuous structure occurs at $\phi = 0.37$. The inverted bicontinuous structure (region 3) is extended to 0.56 water volume fraction. For water volume fractions above 0.56, there is a complete inversion to the oil-in-water microemulsion region. The decrease in dynamic viscosity with the increase in the water volume fractions indicates that the water, which is the least viscous component of the microemulsion system, plays a dominant role in determining the interactions of these systems. Like electrical conductivity, viscosity may also follow scaling type equations in the water-in-oil microemulsion region [47].

$$\eta = A(\phi - \phi_c)^{-\mu} \quad \text{if } \phi > \phi_c \quad (10)$$

$$\eta = B(\phi_c - \phi)^{-s} \quad \text{if } \phi < \phi_c \quad (11)$$

where ϕ is the volume fraction of water, ϕ_c is the percolation threshold, A and B are parameters, and μ and s

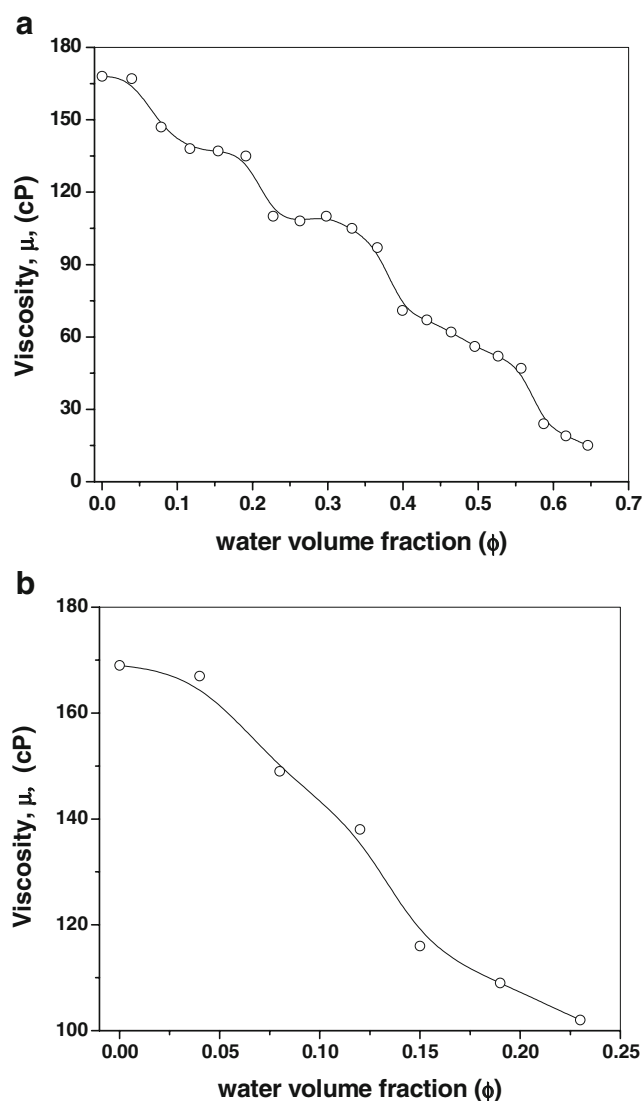


Fig. 3 Variation of the dynamic viscosity (μ) of (water + propylene glycol + sodium chloride)/sucrose laurate/peppermint oil + ethanol system as function of water volume fraction along the dilution line N60 at 25 °C. The mixing ratios (w/w) of water + propylene glycol and that of ethanol/oil equal 2 and 1, respectively. Sodium chloride concentration in water is 0.01 M. The phase diagrams are presented in Fig. 1. The lines serve as guides to the eye. **a** L1695, **b** L595

are scaling exponents. The slopes of the $\log \eta$ versus $\log (\phi_c - \phi)$ plot for $\phi_c > \phi$ and the $\log \eta$ versus $\log (\phi - \phi_c)$ for $\phi > \phi_c$ plot, yield s and μ parameters. The average values of μ and s in Eqs. 10 and 11 are fairly near to the t and s values obtained for conductivity percolation. The estimated scaling parameters which are in good agreement with the experimental values obtained with both electrical conductivity and dynamic viscosity signify that these microemulsion systems show an interdependence of the viscosity–conductivity, especially at the stage of water percolation.

Microstructure parameters

In this section, we measured the small angle X-ray scattering for microemulsion samples, whose compositions lie on the water dilution lines N40, N50, and N60, as shown in the pseudoternary phase diagram of Fig. 1a (L1695 system). In each case, the scattering profile exhibits a single intensity maximum at $q \neq 0$, followed by a high angle tail. Characteristic profiles along the N60 dilution line are presented in Fig. 4. With increasing water content or with a decreasing weight ratio of surfactant to (oil + alcohol), the position of the maximum moves to a lower angle. The width of the peak initially decreases and then increases as a function of water content for N60, whereas for N40 and N50, the peak width continually decreases until the line passes into the two-phase region. For a given water content, the peak width varies inversely with the weight ratio of surfactant to oil + alcohol. We were able to fit (Fig. 4) all the scattering curves to the Teubner–Strey equation [26] (Eq. 1) and to derive the values of periodicity, d , and correlation length, ξ , as described in the “Experimental” section (Eqs. 3 and 4). The dependence of these two parameters on the water volume fraction is plotted in Fig. 5. For the N40 and N50 dilution lines, d increases from 23 to 30 Å and from 24 to 32 Å, respectively, before the two-phase region is entered. Initially, the growth of ξ generally parallels that of d , with the former being smaller than the latter by approximately 16–20 Å. For N60, ξ reaches a maximum at $\phi = 0.23$, while d increases in a monotonic fashion over the whole range of water dilution. The higher values were obtained along the N60 dilution line. The

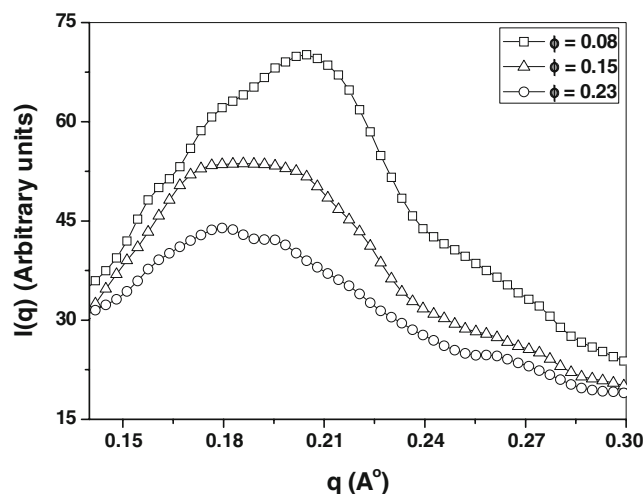


Fig. 4 Small angle X-ray scattering curves for samples whose compositions lie along the dilution line N60 in the water + propylene glycol/L1695/peppermint oil + ethanol microemulsion system at 25 °C. The mixing ratios (w/w) of water/propylene glycol and that of ethanol/oil equal 2 and 1, respectively. The phase diagrams are presented in Fig. 1. The lines serve as guide to the eye

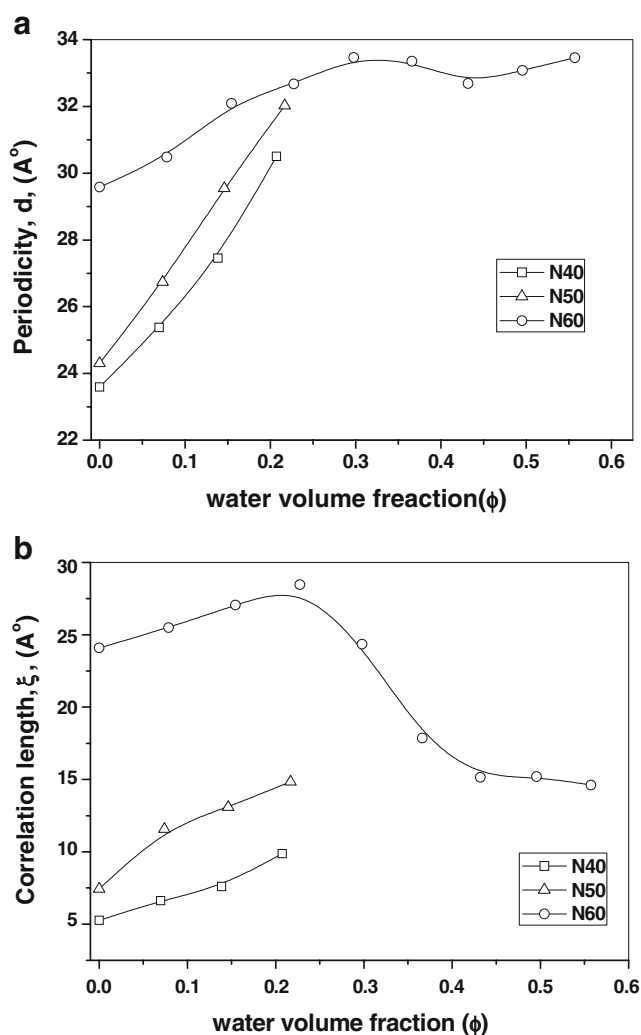


Fig. 5 **a** Periodicity (d) as a function of water volume fraction along the dilution lines N40, N50, and N60 in the water + propylene glycol/L1695/peppermint oil + ethanol system at 25 °C. The mixing ratios (w/w) of water/propylene glycol and that of ethanol/oil equal 2 and 1, respectively. The phase diagram is presented in Fig. 1a. The lines serve as guide to the eye. **b** Correlation length (ξ) of the system presented in **a**

microemulsion system with the higher ξ values is the more ordered. The behavior of the correlation length, ξ , as function of water volume fraction ϕ can be explained as follows: when the water is in the dispersed phase, increasing the water volume fraction increases the size of the scattering units and the correlation length, ξ , whereas when water is in the bulk phase, increasing the water volume fraction dilutes the system and ξ decreases. We also measured the small angle X-ray scattering for microemulsion samples, whose compositions lie on the water dilution line N60 in the L595-based system, as shown in the pseudoternary phase diagram of Fig. 1b (L595 system). In each case, the scattering profile exhibits a single intensity maximum at $q \neq 0$, followed by a high angle tail. Characteristic profiles along the N60 dilution line are presented in Fig. 6a. With increasing water content or with a decreasing weight ratio of surfactant to oil + alcohol, the position of the maximum moves to a lower angle. The width of the peak continually decreases until the line passes into the two-phase region. We were able to fit (Fig. 6a) all the scattering curves to the Teubner–Strey equation [26] (Eq. 1) and to derive the values of the periodicity, d , and correlation length, ξ , as described in the “Experimental” section (Eqs. 3 and 4). The dependence of these two parameters on the water volume fraction is plotted in Fig. 6b. For the L595, d increases from 30 to 33 Å before the two-phase region is entered. The growth of ξ generally parallels that of d , with the former being smaller than the latter by approximately 17 Å. For L595, d values are higher than those observed with the L1695 for the same water

teristic profiles along the N60 dilution line are presented in Fig. 6a. With increasing water content or with a decreasing weight ratio of surfactant to oil + alcohol, the position of the maximum moves to a lower angle. The width of the peak continually decreases until the line passes into the two-phase region. We were able to fit (Fig. 6a) all the scattering curves to the Teubner–Strey equation [26] (Eq. 1) and to derive the values of the periodicity, d , and correlation length, ξ , as described in the “Experimental” section (Eqs. 3 and 4). The dependence of these two parameters on the water volume fraction is plotted in Fig. 6b. For the L595, d increases from 30 to 33 Å before the two-phase region is entered. The growth of ξ generally parallels that of d , with the former being smaller than the latter by approximately 17 Å. For L595, d values are higher than those observed with the L1695 for the same water

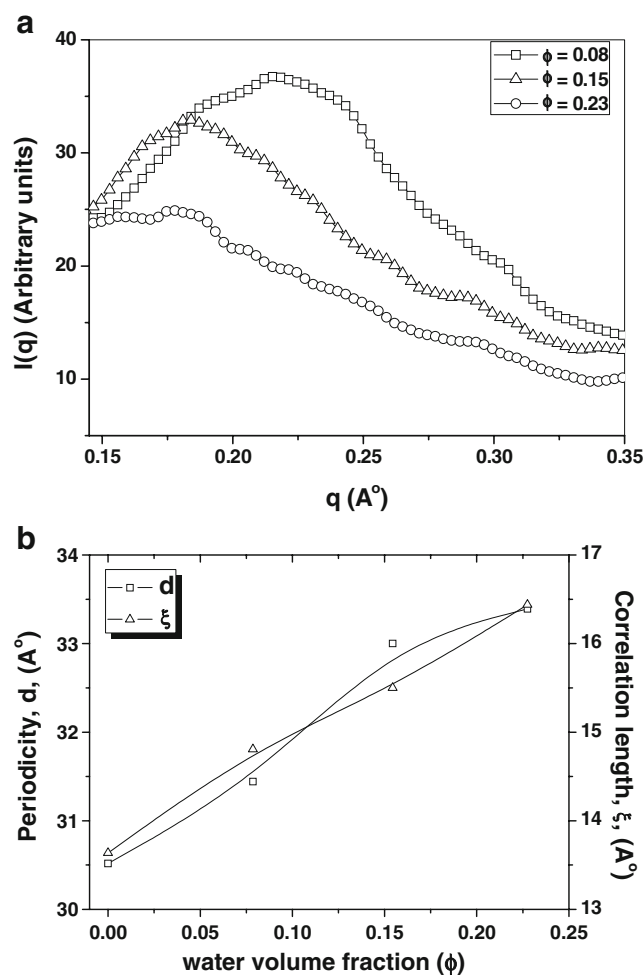


Fig. 6 **a** Small angle X-ray scattering curves for samples whose compositions lie along the dilution line N60 in the water + propylene glycol/L595/peppermint oil + ethanol microemulsion system at 25 °C. The mixing ratios (w/w) of water/propylene glycol and that of ethanol/oil equal 2 and 1, respectively. The phase diagrams are presented in Fig. 1. The lines serve as guide to the eye. **b** Periodicity (d) and correlation length (ξ) for the system presented in **a**

volume fractions, while ξ values are lower. The difference in the behavior of microstructure parameters d and x between L595 and L1695 is explained in the following way: Formation of the microemulsions using the hydrophilic surfactant L1695 will increase the solubility of the surfactant in the aqueous phase and enhance water solubilization. L1695 increases the available interface and results in a higher number of micelles with shrinking size. Upon using L1695, the effective volume fractions of the dispersed phase remain nearly constant, while the interaction radii of the micelles decrease. L1695 reduces the size of the micelles, which is in good agreement with the shrinking interaction radii derived from the structure factor. Consequently, the number of particles per unit volume is lowered, but these fewer particles have a stronger scattering power. At the same time, the effective volume fraction of interaction stays approximately the same in the presence of L1695, which, in combination, implies that the number of micelles per unit volume and, therefore, also the available interface must be increased.

Diffusion parameters

In order to evaluate the diffusion data in terms of microstructure, the calculation of the relative diffusion coefficient, D/D_0 , of the oil and water is needed [48–54]. Relative diffusion coefficients were obtained by dividing water (D^{Water}) and oil (D^{Oil}) diffusion coefficients in the microemulsion by the diffusion coefficient of pure water (D_0^{Water}) and oil in the neat phase (D_0^{Oil}). It is well documented [48–54] that if the D/D_0 values of water and oil differ by more than 1 order of magnitude, discrete particles of the slowly diffusing solvent are implied, whereas if the D/D_0 values of water and oil are of the same order of magnitude, a bicontinuous structure is suggested. Figure 7a shows the relative diffusion coefficients of water and peppermint oil in water + propylene glycol/L1695/peppermint oil + ethanol microemulsion system as a function of the water content (weight percent) along the dilution line N60 (Fig. 1a). One can clearly see that the general diffusion coefficient behaviors of microemulsion ingredients [oil and water] at the two extremes of aqueous phase concentrations (below 0.2 and above 0.70 wt.% water contents), the $D^{\text{Water}}/D_0^{\text{Water}}$ values are easily interpreted, while the in-between regions are somewhat more difficult to explain since gradual changes take place. As Fig. 7a indicates, microemulsions containing below 0.20 water volume fraction have a discrete water-in-oil microstructure, since the relative diffusion coefficients of water and peppermint oil differ by more than 1 order of magnitude. Microemulsions containing 0.20–0.56 water volume fraction have a bicontinuous microstructure, as the diffusion coefficients of water and peppermint oil are of the

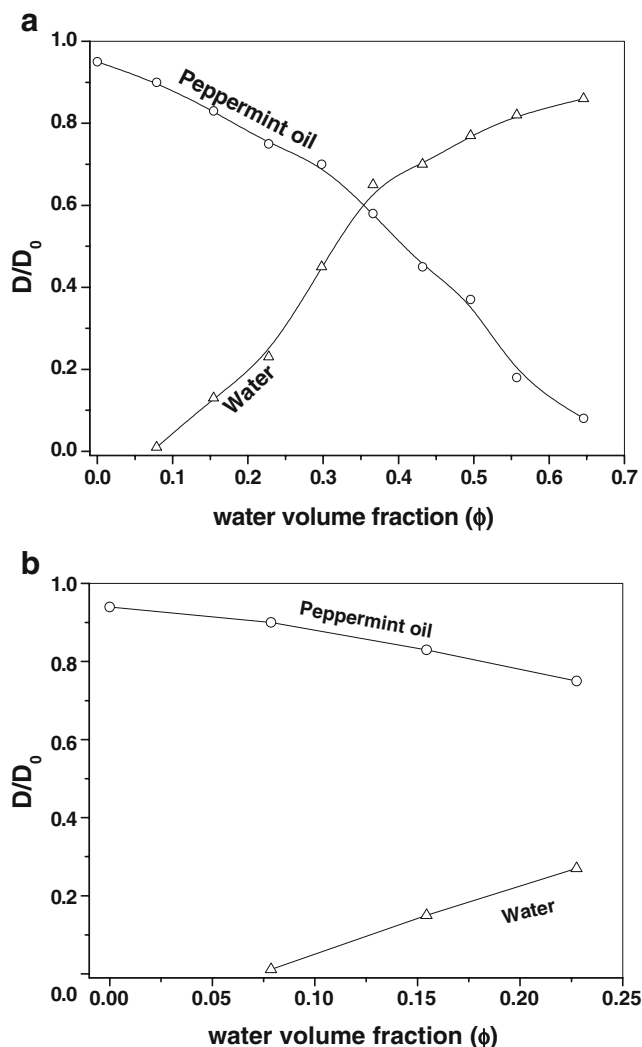


Fig. 7 Relative diffusion coefficients of water (Δ) and peppermint oil (O) for samples whose compositions lie along the dilution line N60 in the water + propylene glycol/sucrose laurate/peppermint oil + ethanol microemulsion system at 25 °C. The mixing ratios (w/w) of water/propylene glycol and that of ethanol/oil equal 2 and 1, respectively. The phase diagrams are presented in Fig. 1. The lines serve as guide to the eye. **a** L1695, **b** L595

same order of magnitude. Increasing the aqueous phase concentration to above 0.56 water volume fraction induces the formation of discrete oil-in-water microstructure. Figure 7b presents the relative diffusion coefficients of peppermint oil and water in the water + propylene glycol/L595/peppermint oil + ethanol system. The diffusion trends of peppermint oil and water are not very different from those in the L1695-based system. It can also be seen that for all water volume fractions below the $D^{\text{Water}}/D_0^{\text{Water}}$ and $D^{\text{Oil}}/D_0^{\text{Oil}}$ indicate the presence of water-in-oil microemulsions. As Fig. 7 indicates, it is clear that hydrophilicity of the surfactant affects the diffusion properties of both water and oil. The observed diffusion coefficients of L1695 and L595 are plotted in Fig. 8. The observed diffusion

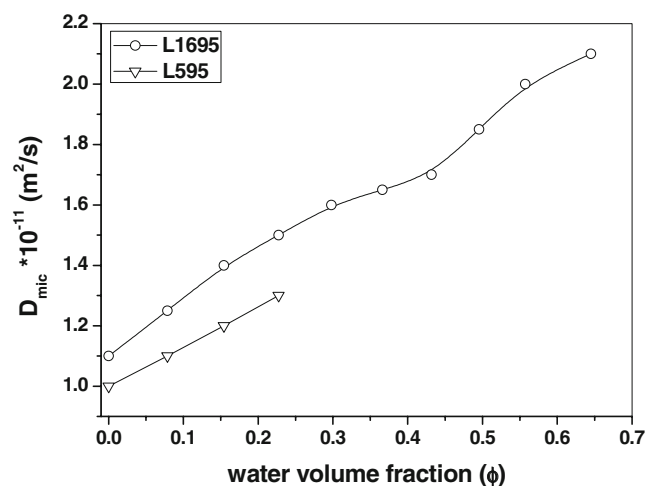


Fig. 8 Diffusion coefficients of surfactants for samples whose compositions lie along the dilution line N60 in the water + propylene glycol/sucrose laurate/peppermint oil + ethanol microemulsion system at 25 °C. The mixing ratios (w/w) of water/propylene glycol and that of ethanol/oil equal 2 and 1, respectively. The phase diagrams are presented in Fig. 1. The lines serve as guide to the eye

coefficient of the L1695 (D^{L1695}) is related to the self-diffusion coefficients of the aggregated and the free molecules, D_{mic}^{L1695} and D_{free}^{L1695} , respectively, by

$$D^{L1695} = p_{mic} D_{mic}^{L1695} + (1 - p_{mic}) D_{free}^{L1695} \quad (12)$$

where D^{L1695} denotes the L1695 experimental self-diffusion coefficient, and D_{mic}^{L1695} and D_{free}^{L1695} represent the translational self-diffusion coefficient of micellized L1695 surfactant, respectively. The measured value of D_{mic}^{L1695} is $1.28 \times 10^{-11} \text{ m}^2/\text{s}$ at 0.1 water volume fraction. The diffusion coefficient of free sucrose laurate D_{free}^{L1695} is $1 \times 10^{-10} \text{ m}^2/\text{s}$. p_{mic} is the fraction of micellized surfactant which equals $1 - \text{CMC}/c$, where c is the overall mixed surfactant concentration. For the high surfactant content of the present study, the contribution from free surfactant molecules is negligible because the CMC of L1695 is very low ($1 \times 10^{-5} \text{ M}$ at 25 °C). Hence, increasing L1695 diffusion coefficient with increasing water concentration reflects micellar growth [48–54].

Hydrodynamic radius and area per polar head group

In this section, we used the dynamic light scattering technique to investigate the water + propylene glycol/L1695/peppermint oil + ethanol microemulsion systems as a function of temperature at aqueous contents equal 0.56 and 0.65 water volume fractions along the dilution line N60. The values of the hydrodynamic radius increase with temperature increase indicating that the micelles grow in size as the temperature increases and a change may occur on the shape in the micelles, that is, sphere to rod or sphere to disk transitions. The microemulsion droplets deform by thermal fluctuations. The droplets may undergo attractive

interactions that lead to aggregation between the droplets. Two mechanisms have been used to explain the origin of the attractive interactions: interpenetration of the tails of the surfactants molecules residing on different droplets or fusion of droplets which lowers the curvature energy. Similar results of the behavior of the hydrodynamic radius as a function of temperature were reported in our previous studies [8, 55, 56]. Assuming spherical aggregates with no oil penetration into the mixed surfactants film, the area per polar head group (a) can be estimated from the R_H and the ratio of the volume fraction of oil to the volume fraction of L1695 (ϕ_O/ϕ_S) is determined by the relation [57]

$$a = \frac{3v_s}{R_H} \left(1 + \frac{\phi_O}{\phi_S} \right) \quad (13)$$

where v_s is the L1695 molecular volume which equals 720 \AA^3 . R_H is the hydrodynamic radius. The values of the area per polar head group (a) and the hydrodynamic radius for aqueous phase volume fractions equal 0.56 and 0.65 are presented in Table 2.

Conclusions

We studied the microemulsion systems based on sucrose ester surfactants and the biocompatible peppermint oil. We estimated the maximum water solubilization and the thermodynamics of solubilization of either water-in-oil or oil-in-water. These systems are promising for many industrial applications including drug delivery, solubilization of food functional ingredients, medium for biochemical reactions, and nanoparticle synthesis. From this study, we were able to draw the following conclusions:

- The electrical conductivities and dynamic viscosities of the systems reveal the occurrence of percolative structures at low values of water fractions. This percolation phenomenon is static indicating that the

Table 2 The values of the area per polar head group (a) and the hydrodynamic radius for aqueous phase volume fractions equal 0.56 and 0.65 of the water + propylene glycol/L1695/peppermint oil + ethanol microemulsion system at 25 °C along the N60 dilution line

Temperature (°C)	Water volume fraction (φ)			
	0.56		0.65	
	R_H (nm)	a (\AA^2)	R_H (nm)	a (\AA^2)
20	2.4	154	2.2	147
25	2.7	137	2.5	130

The mixing ratios (w/w) of water/propylene glycol and that of ethanol/oil equal 2 and 1, respectively.

percolative structures are transferred to bicontinuous structures.

- The periodicity of microemulsions increases linearly with the increase in the water volume fraction indicating monodimensional swelling of the microemulsions droplets.
- The correlation length of the microemulsions increases with the increase on the water volume fraction up to a certain value then decreases indicating that when the water is in the dispersed phase, increasing the water volume fraction increases the size of the scattering units and the correlation length, ξ , whereas when water is in the bulk, increasing the water volume fraction dilutes the scattering units and ξ decreases.
- The measured microstructure parameters in these systems by small angle X-ray scattering demonstrate that the L595-based microemulsions are less ordered than those based on L1695 which indicates that the hydrophilicity of the surfactant controls the degree of order of the formulated microemulsions.
- The picture that emerges from the data over the whole water content range studied is that at low water content values there are probably spherical droplets of water-in-oil. As the water content increases, the water-in-oil microstructure is no longer optimal and a flattening of the interfacial film is approached. Both water and oil diffusing rapidly indicates an average equilibrium bicontinuous arrangement where neither oil nor water is confined into closed domains. Both oil and water have lower relative diffusion coefficients in the L1695-based microemulsions compared to the L595-based one.
- The area per polar head group decreases with the increase of temperature.

References

1. Fanun M (ed) (2008) Microemulsions: properties and applications. Taylor and Francis/CRC, Boca Raton
2. Kumar P, Mittal KL (eds) (1998) Handbook of microemulsions science and technology. Marcel Dekker, New York
3. Sjöblom J, Lindberg R, Friberg SE (1996) Microemulsions-phase equilibria characterization, structure, applications and chemical reactions. Adv Colloid Interface Sci 95:125–287
4. Moulik SP, Paul BK (1998) Structure, dynamics and transport properties of microemulsions. Adv Colloid Interface Sci 78:99–195
5. Solans C, Kunieda H (eds) (1997) Industrial applications of microemulsions. Surfactant science series Vol. 66. Marcel Dekker, New York
6. Fanun M (2008) A study of the properties of mixed nonionic surfactants microemulsions by NMR, SAXS, viscosity and conductivity. J Mol Liq 142:103–110
7. Fanun M (2007) Conductivity, viscosity, NMR and diclofenac solubilization capacity studies of mixed nonionic surfactants microemulsions. J Mol Liq 135:5–13
8. Fanun M, Salah Al-Diyn W (2007) Structural transitions in the system water/mixed nonionic surfactants/R (+)-limonene studied by electrical conductivity and self-diffusion-NMR. J Dispers Sci Technol 28:165–174
9. Kunieda H, Ozawa K, Huang KL (1998) Effect of oil on the surfactant molecular curvatures in liquid crystals. J Phys Chem B 102:831–837
10. Aramaki K, Kunieda H (1999) Solubilization of oil in a mixed cationic liquid crystal. Colloid Polym Sci 277:34–40
11. Glatter O, Orthaber D, Stradner A, Scherf G, Fanun M, Garti N, Clement V, Leser ME (2001) Sugar ester non-ionic microemulsions: structural characterization. J Colloid Interface Sci 241:215
12. Fanun M, Wachtel E, Antalek B, Aserin A, Garti N (2001) A study of the microstructure of four-component sucrose ester microemulsions by SAXS and NMR. Colloids Surf A 180:173–186
13. Lehmann L, Keipert S, Gloor M (2001) Effects of microemulsions on the stratum corneum and hydrocortisone penetration. Eur J Pharm Biopharm 52:129–136
14. Zhang H, Feng F, Fu X, Du Y, Zhang L, Zheng X (2007) Antimicrobial effect of food-grade GML microemulsions against *Staphylococcus aureus*. Eur Food Res Technol 226:281–286
15. Garti N, Clement V, Fanun M, Leser ME (2000) Some characteristics of sugar ester nonionic microemulsions in view of possible food applications. J Agric Food Chem 48:3945–3956
16. Khiew PS, Huang NM, Radiman S, Ahmad S (2004) Synthesis of NiS nanoparticles using a sugar-ester nonionic water-in-oil microemulsion. Mater Lett 58:762–767
17. Kahlweit M, Strey R, Busse G (1990) Microemulsions: a qualitative thermodynamic approach. J Phys Chem 94:3881–3894
18. Kahlweit M, Strey R, Schomacker R, Hasse D (1989) General patterns of the phase behavior of mixtures of water, nonpolar solvents, amphiphiles, and electrolytes. 2. Langmuir 5:305–315
19. Schubert KV, Kaler E (1996) Nonionic microemulsions. Ber Bunsenges Phys Chem 100:190
20. Kahlweit M, Strey R, Haase D, Kunieda H, Schmeling T, Faulhaber B, Borkovec M, Eicke HF, Busse G, Eggers F, Funck T, Richmann H, Magid L, Soderman O, Stilbs P, Winkler J, Dittich A, Jahn W (1987) How to study microemulsions? J Colloid Interface Sci 118:436–453
21. Berghenoltz J, Romagnoli A, Wagner N (1995) Viscosity, microstructure, and interparticle potential of AOT/H₂O/n-decane inverse microemulsions. Langmuir 1:1559–1570
22. Feldman Y, Kozlovich N, Nir I, Garti N (1995) Dielectric relaxation in sodium bis(2-ethylhexyl) sulfosuccinate–water–decane microemulsions near the percolation temperature threshold. Phys Rev E 51:478–491
23. Cametti C, Codastefano P, Tartaglia P, Chen SH, Rouch J (1992) Electrical conductivity and percolation phenomena in water-in-oil microemulsions. J Phys Rev A 45:R5358–R5361
24. Eicke HF, Meier W, Hammerich H (1994) On electric conductivity of infinite clusters in water-in-oil microemulsions. Langmuir 10:2223–2227
25. Lake JA (1967) An iterative method of slit-correcting small angle X-ray data. Acta Crystallogr A 23:191–194
26. Teubner M, Strey R (1987) Origin of the scattering peak in microemulsions. J Chem Phys 87:3195
27. Teukolsky SA, Vetterling WT, Flannery BP (1992) Numerical recipes in C: the art of scientific computing. Cambridge University Press, New York
28. Brunner-Popela J, Mittelbach R, Strey R, Schubert KV, Kaler EW, Glatter O (1999) Small-angle scattering of interacting particles. III. D2O-C12E5 mixtures and microemulsions with n-octane. J Chem Phys 21:10623

29. Wu D, Chen A, Johnson CS (1995) An improved diffusion-ordered spectroscopy experiment incorporating bipolar-gradient pulses. *J Magn Reson* 115:260–264
30. Stejskal EO (1995) In: Stejskal EO (ed) *Encyclopedia of nuclear magnetic resonance*. Wiley, New York, pp 657–658
31. Koppel DE (1972) Analysis of macro molecular polydispersity in intensity correlation spectroscopy: the method of cumulants. *J Chem Phys* 57:4814–4820
32. Provencher SW (1979) Inverse problems in polymer characterisation: direct analysis of polydispersity with photon correlation spectroscopy. *Macromol Chem* 180:201–209
33. Pes MA, Aramaki K, Nakamura N, Kunieda H (1996) Temperature-insensitive microemulsions in a sucrose monoalkanoate system. *J Colloid Interface Sci* 178:666
34. Fanun M (2009) Microemulsion formation on water/nonionic surfactant/peppermint oil mixtures. *J Dispers Sci Technol* 30 (3):289–296
35. Strey R (1996) I. Experimental facts water-nonionic surfactant systems, the effect of additives. *Ber Bunsenges Phys Chem* 100:182–189
36. Yaghmur A, Aserin A, Garti N (2002) Phase behavior of microemulsions based on food-grade nonionic surfactants: effect of polyols and short-chain alcohols. *Colloids Surf A* 209:71–81
37. Garti N, Aserin A, Fanun M (2000) Non-ionic sucrose esters microemulsions for food applications, part I: Water solubilization. *Colloids Surf A* 164:27–38
38. Stilbs P, Lindman B (1983) Effect of alcohol cosurfactant length on microemulsion structure. *J Colloid Interface Sci* 95:583–585
39. Alany RG, Rades T, Agatonovic-Kustin S, Davies NM, Tucker IG (2000) Effects of alcohols and diols on the phase behaviour of quaternary systems. *Int J Pharm* 196:141
40. Safran SA, Grest GS, Bug A, Webman I (1987) I. Percolation in interacting microemulsions. In: Rosano H, Clausse M (eds) *Microemulsion systems*. Marcel Dekker, New York, pp 235–245
41. De Gennes PG, Taupin C (1990) Microemulsions and the flexibility of oil/water interfaces. *J Phys Chem* 94:8407–8413
42. Grest G, Webman I, Safran S, Bug A (1986) Dynamic percolation in microemulsions. *Phys Rev A* 33:2842–2845
43. Djordjevic L, Primorac M, Stupar M, Krajisnik D (2004) In vitro release of diclofenac diethylamine from caprylocaproyl macroglycerides based microemulsions. *Int J Pharm* 271:11–19
44. Mehta SK, Dewan RK, Bala K (1994) Percolation phenomenon and the study of conductivity, viscosity, and ultrasonic velocity in microemulsions. *Phys Rev E* 50:4759–4762
45. Ajith S, Rakshit AK (1995) Effect of NaCl on a nonionic surfactant microemulsion system. *Langmuir* 11:1122–1126
46. Rakshit AK, Ajith S (1995) Studies of mixed surfactant microemulsion systems: Brij 35 with Tween 20 and sodium dodecyl sulfate. *J Phys Chem* 99:14778–14783
47. Peyrelasse J, Boned C (1990) Conductivity, dielectric relaxation, and viscosity of ternary microemulsions: the role of the experimental path and the point of view of percolation theory. *Phys Rev A* 41:938–953
48. Nilsson PG, Lindman B (1983) Water self-diffusion in nonionic surfactant solution. Hydration and obstruction effects. *J Phys Chem* 87:4756–4761
49. Lindman B, Shinoda K, Jonstromer M, Shinohara A (1988) A change of organized solution (microemulsion) structure with small changes in surfactant composition as revealed by NMR self-diffusion studies. *J Phys Chem* 92:4702–4706
50. Bastogne F, Nagy BJ, David C (1999) Quaternary ‘N-alkylaldonamide-brine-decane-alcohol’ systems. Part II: microstructure of the one-phase microemulsion by NMR spectroscopy. *Colloids Surf A* 148:245–257
51. El-Seoud O (1997) Use of NMR to probe the structure of water at interfaces of organized assemblies. *J Mol Liq* 72:85–103
52. Olsson U, Nagai K, Wennerstrom H (1988) Microemulsions with nonionic surfactants. 1. Diffusion process of oil molecules. *J Phys Chem* 92:6675–6679
53. Soderman O, Nyden M (1999) NMR in microemulsions. NMR translational diffusion studies of a model microemulsion. *Colloids Surf A* 158:273–280
54. Ko CJ, Ko YJ, Kim DM, Park HJ (2003) Solution properties and PGSE-NMR self-diffusion study of $C_{18:1}E_{10}$ /oil/water system. *Colloids Surf A* 216:55–63
55. Fanun M (2007) Structure probing of water/mixed nonionic surfactants/caprylic capric triglyceride. *J Mol Liq* 133:22–27
56. Fanun M, Salah Al-Diyn W (2006) Electrical conductivity and self diffusion NMR studies of the system: water/sucrose laurate/ethoxylated mono-di-glyceride/isopropylmyristate systems. *Colloids Surf A* 277:83–89
57. Arvidsson A, Soderman O (2001) The microemulsion phase in the didecyltrimethylammonium bromide/dodecane/water system. Phase diagram, microstructure, and nucleation kinetics of excess oil phase. *Langmuir* 17:3567–3572